Electron beam lithography on non-planar, suspended, 3D AFM cantilever for nanoscale thermal probing

R Swami, G Julié, D Singhal, J Paterson, J Maire, S Le-Denmat, J Motte, S Gomès, O Bourgeois

Electron Beam Lithography on Non-planar, Suspended, 3D AFM Cantilever for Nanoscale Thermal Probing

R. Swami,[1,2] G. Julié,[1,2] D. Singhal,[1,2] J. Paterson,[1,2] J. Maire,[1,2]
S. Le-Denmat,[1,2] J.F. Motte,[1,2] S. Gomès,[3] and O. Bourgeois[1,2]

[1] *Institut NÉEL, CNRS, 25 avenue des Martyrs, F-38042 Grenoble, France*

[2] *Univ. Grenoble Alpes, Inst NÉEL, F-38042 Grenoble, France*

[3] *CETHIL - Centre d'Energétique et de Thermique de Lyon, CNRS, 9 Rue de la Physique, 69621 Villeurbanne, France*

(Dated: May 17, 2022)

Abstract

Electron beam lithography (EBL) on non-planar, suspended, curved or bent surfaces is still one of the most frequently stated problems for fabricating novel and innovative nano-devices and sensors for future technologies. Although spin coating is the most widespread technique for electron resist (e-resist) deposition on 2D or flat surfaces, it is inadequate for suspended and 3D architectures because of its lack of uniformity. In this work, we use a thermally evaporated electron sensitive resist the QSR-5 and study its sensitivity and contrast behaviour using EBL. We show the feasibility of utilizing the resist for patterning objects on non-planar, suspended structures via EBL and dry etching processes. We demonstrate the integration of metal or any kind of thin films at the apex of an atomic force microscopy (AFM) tip. This is showing the great potential of this technology in various fields, such as magnetism, electronic, photonics, phononics and other fields related to near field microscopy using AFM probe like for instance scanning thermal microscopy.

INTRODUCTION

Fields of energy [1–3], micro- and nano-electronics [4], fundamental study of quantum effects [5] and lab-on-chip technologies [6] require innovative and effective nanofabrication strategies. Electron beam lithography (EBL) [7] is the most widely employed method in the growth of novel technologies for research and development as well as for prototyping devices at the nanoscale. The ongoing trend in nanotechnology of fabricating nanostructures on non-planar 3D architectures has shown significant potential in various fields. Well-known examples are magnetic force microscopy [8, 9], tip-enhanced Raman spectroscopy [10], near-field optical focusing [11], scanning single-electron transistor microscopy [12] and scanning thermal microscopy (SThM)[13–25] that demand nanofabrication on 3D AFM probes. Recently, a considerable amount of literature has been published on EBL for creating nanostructures on irregular surfaces [26–38]. However, it is still very challenging to perform EBL on non-planar, 3D architectures because of the lack of uniformity and reproducibility of electron sensitive resist (e-resist) films on the substrates.

Spin coating is the most widely used method for resist deposition to structure materials and devices in scientific laboratories, as well as in the micro- and nano-electronics industry. One of the key issue of this method is its inhomogeneities of film thickness on non-planar, suspended, and 3D substrates, which is due to the presence of edge-bead effects. On the

contrary, it has been reported that e-resist with low-viscosity and low-surface-tension can be coated on non-planar surfaces [26] by spin coating. Besides spin coating, various other methods have been demonstrated to deposit resist films on non-planar surfaces such as spray coating [27], Langmuir-Blodgett (LB) technique [28], float coating [8], monolayer brush [29–31], dip coating [30, 32] and ice lithography (IL) [33–36]. However, most of these methods exhibit some major issues such as non-uniformity, ultra thin-films, reproducibility and extremely low sensitivity.

Therefore, in this work, we used a vacuum based thermal evaporation system [39] to deposit the QuantiScript 5 (QSR-5) e-resist, a negative resist where the cross-linking is activated by the energy of the electron beam. To date, the thermal evaporation method is the most efficient way for coating a uniform layer of resist on non-planar, bent, suspended, irregular surfaces or 3D architectures [37, 38, 40]. We first calibrate the deposition for the QSR-5 resist on planar and non-planar substrates. Then we perform the state-of-the-art EBL and show that lines structures with spatial resolution of 100 nm can be readily made on a regular flat surface. Moreover, we study the impact of developers on the electron exposure dose during the lithographic process using QSR-5D2 and methyl ethyl ketone (MEK) developers. We then apply this process on a highly non-planar geometry, namely a 3D AFM probe consisting of a cantilever whose tip is surmounted by a hollow pyramid 3 μm in height. We pattern 800 nm wide gold strips on a pyramid-shaped AFM tip. Finally, we demonstrate the integration of niobium nitride (NbN) resistive thermometer thin film at the apex of a 3D AFM tip and gold thin film on the cantilever dedicated to advanced near field microscopy for nanoscale thermal measurements.

METHODS

The aim of the present work is to demonstrate patterning of thin film on non-planar suspended 3D architectures by employing unconventional nanofabrication strategies. The ultimate scientific goal is to pattern thin film of resistive materials on an AFM cantilever that will serve as thermometer for scanning thermal microscopy, a well-known near field microscopy technique for mapping temperature or thermal conductivity at sub-50 nm spatial resolution [13–25, 41].

In that respect, we use commercial SiN AFM probes OTR8-10 having low thermal

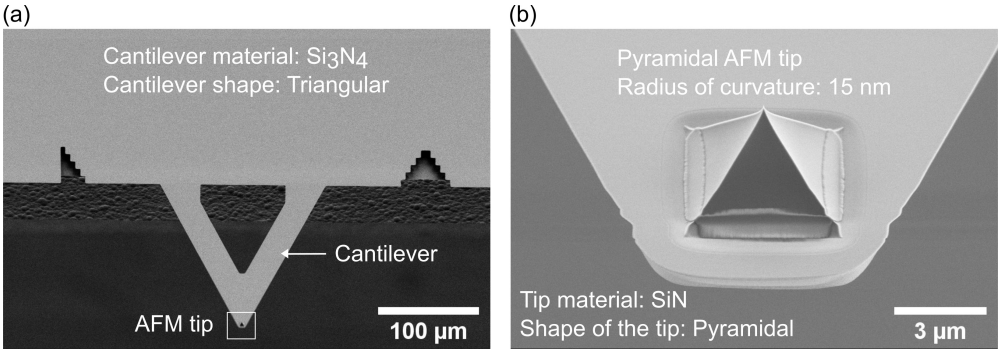

FIG. 1. SEM images of commercial AFM probes OTR8-10 used in the fabrication process [42]. (a) Top-view of the AFM probe with the triangular-shaped cantilever and tip. (b) Close-up SEM micrograph of the pyramidal-shaped AFM tip with radius of curvature about 15 nm and height of 3 μm.

conductivity and electrical insulating properties perfectly adapted for fabricating a highly sensitive probe of temperature, as can be seen from Figure 1 [42]. These probes have triangular-shaped cantilevers and pyramidal-shaped tips with a tip height of 2.5 to 3.5μm. The length and width of these cantilevers are in microns and apex of the tip has a radius of curvature about 15 nm. To structure a thin film on a non-planar 3D surface like an AFM probe, we used a process based on electron sensitive QSR-5 resist that can be thermally evaporated on suspended structures along with state-of-the-art nano-structuration techniques including EBL, sputtering and dry etching processes tools such as reactive ion etching (RIE) and physical ion beam etching (IBE).

In this work, we use the QSR-5 negative e-beam sensitive resist that can be thermally evaporated on suspended structures for two main reasons 1-the resist can be deposited without spinning process making it perfectly adpated for very small samples and 2-using evaporated e-beam resist avoids having edge bead effects, detrimental to the quality of the electron beam lithography. The QSR-5 is composed of a powder of sterol chain, very stable at room temperature, having a melting point above 100 $^\circ$C perfectly appropriate to vapour deposition onto a target substrate. When exposed to electron beam energy sources, double bonds between carbon atoms in cyclic structure sterols are broken down allowing cross link reaction [43]. The exposed part of the QSR-5 will remain as the non-exposed part will be washed out by the developer such as QSR-5D2 and MEK.

We first study the properties of the thermally evaporated QSR-5 e-resist on planar

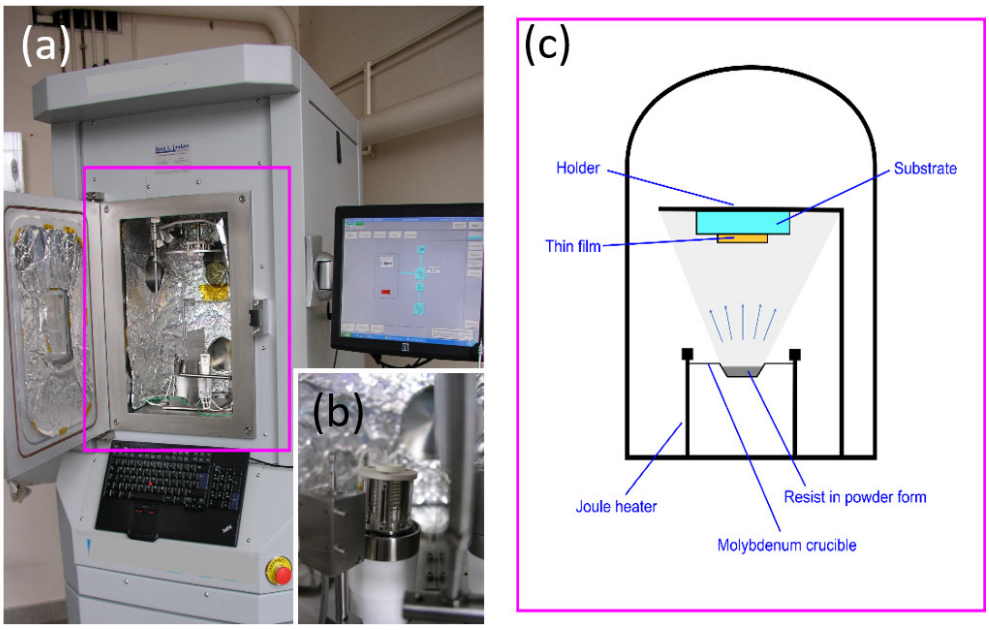

FIG. 2. (a) and (b) are respectively the photograph of the thermal evaporator instrument and the evaporation crucible. (c) The schematic represents the simplified view of the thermal evaporation process. The QSR-5 resist (in powder form) is placed in molybdenum crucible (b) and Joule effect is utilized to increase the temperature of the crucible for evaporating the resist with desired rates.

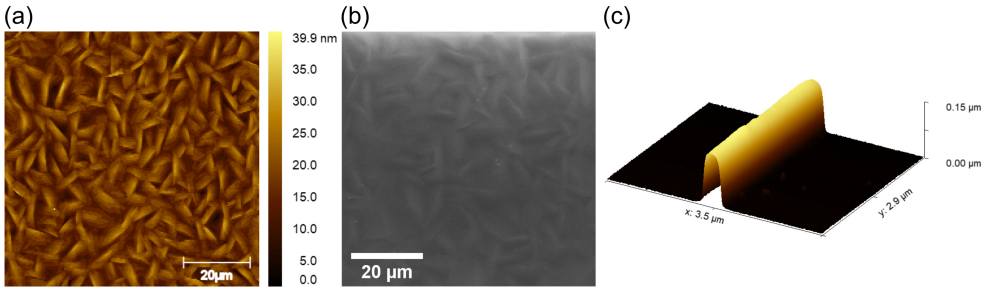

FIG. 3. (a) AFM image and (b) SEM image of a QSR-5 e-resist film with a thickness of 170 ±15 nm evaporated on SiN substrate where the rice grain structures can be distinguished. (c) Topographic 3D AFM image of patterned QSR-5 (yellow, false colour shows e-resist step).

substrates. This includes probing the effect of surface roughness, sensitivity, contrast of the resist along with the investigation of the impact of the various resist developers on the optimal electron exposure dose to be used during a lithography process.

The deposition of QSR-5 e-resist is performed using a thermal evaporator based on Joule effect with an initial base chamber pressure of 2×10^{-7} mbar as shown in Figure 2. During

the deposition, the temperature of the molybdenum crucible (see Figure 2(b)) containing the QSR-5 powder is increased gradually up to 130°C until the desired evaporation rate of 1 Å.s^{-1} is achieved. After the deposition of resist, the sample is covered in aluminium foil for 24 hours to ensure adequate adhesion. Note that to obtain a high quality resist film, low base pressure and low evaporation rate are required. Figure 3 (a) and (b) represents the AFM and SEM images of evaporated QSR-5 resist film on a commercially polished SiN (100 nm) film on bulk Si substrate. A microscopic rice grain structure is observed with a mean roughness of 15 nm, measured by AFM. However, this granular structure and high roughness of the resist film does not play a critical role in the patterning of QSR-5 resist, as it can been seen from the 3D topographic AFM image in Figure 3 (c) showing that clean lines of width 0.5 μm can be structured using electron beam lithography.

To assess the sensitivity and contrast behaviour of the QSR-5 resist, EBL is carried out using a LEO-1530 field emission SEM system. The arrays of lines (length×width: 20 μm×(50 to 500 nm)) are exposed at an accelerating voltage of 5 keV with an electron dose range of 1 to 3000 μC.cm^{-2} on e-resist grafted on different surfaces, including e-gun evaporated Au film and commercial SiN substrate. The exposed samples are developed by immersion, either in QSR-5D2 developer for 12 minutes or MEK for 1.5 minutes at 30 °C. Afterwards, the mean remaining thickness of the exposed resist is estimated. In order to do so, the height difference between the unexposed and exposed area is measured using AFM, and the subtraction between them provides the remaining resist thickness (see Figure 3(c)). The topographic AFM images and corresponding height profiles of patterned QSR-5 resist on Au and SiN surfaces are represented in Figure 4 (a). The exposure dose used to create these patterns is kept constant for each set, while the width of rectangles is increased from 50 nm to 500 nm (right to left). From the topography images and profile of resist in Figure 4(a) (1-4), it is apparent that the rightmost patterns of width 50 nm are barely visible.

Figure 4 (b) and (c) compare the contrast curves for QSR-5 resist exposed at 5 keV and developed either in QSR-5D2 or MEK for rectangles of length×width: 20 μm×500 nm. The curves of the contrast γ describe the sharpness of the resist profile as a function of exposure dose, where γ is defined as $\gamma = [\log(D_{100}/D_0)]^{-1}$, D_0 is the maximum electron dose at which the resist does not exposed and D_{100} is the minimum dose to fully exposed the resist (over all the thickness). The term D_{100} is also refering to the sensitivity of the resist. The contrast γ for the QSR-5 resist grafted on Au surface and developed in QSR-5D2 and MEK are 0.7

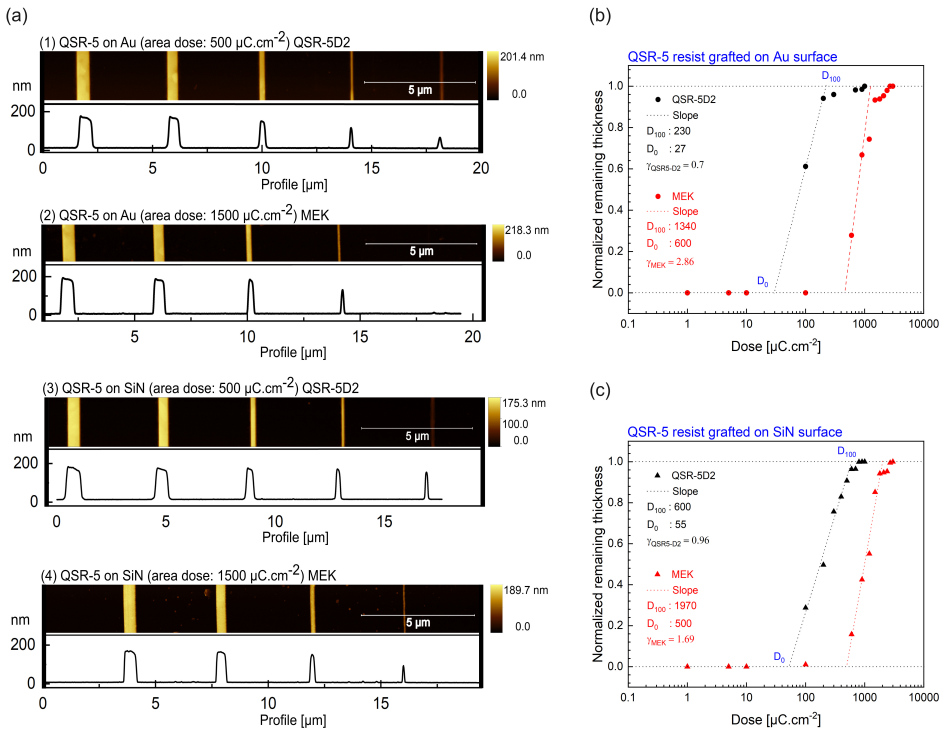

FIG. 4. (a) Topographic AFM images and corresponding height measurements of patterned QSR-5 resist on Au and SiN surfaces. The exposure was carried out at 5keV, and developed at 30 °C either in QSR-5D2 developer for 12 minutes or in MEK for 1.5 minutes. (a)-1 array of rectangles (length×width: 20 μm×(50 to 500 nm)) of QSR-5 resist patterned on a Au surface, with the exposure dose of 500 μC.cm^{-2}, developed in QSR-5D2 and (a)-2 the exposure dose of 1500 μC.cm^{-2} and developed in MEK. (a)-3 shows the patterned QSR-5 on SiN exposed at 500 μC.cm^{-2} and developed in QSR-5D2. (a)-4 the exposure is performed at 1500 μC.cm^{-2} and developed in MEK. (b) and (c) represents the contrast curves of the QSR-5 resist exposed at 5 keV for rectangles of length×width: 20 μm×500 nm and the impact of developers is shown on the electron exposure dose. (b) QSR-5 thin film grafted on Au surface (solid dots), and (c) SiN surface (solid triangles) are developed in QSR-5D2 and MEK. D_0 is the maximum electron dose at which the resist does not exposed and D_{100} is the minimum dose to fully (100 %) exposed the resist (over all the thickness).

and 2.86 respectively. In the case of resist grafted on SiN surface, the contrast is 0.96 for QSR-5D2 and 1.69 for MEK developer. Higher doses are requireed when working on SiN as compared to Au because the atomic number and the density of SiN is much smaller than for Au. Indeed, from SiN surfaces less electrons will be backscattered in the resist as compared

to Au surface reducing the exposure of the resist to electrons.

From the graph of Figure 4 (b) and (c), it is interesting to note that the contrast as well as the sensitivity of the resist are depending on the way the surfaces are grafted. The optimized electron dose to expose the resist on Au and SiN surfaces are found to be 230 and 600 μC.cm^{-2} respectively. In addition, the contrast tends to be higher in MEK developer because of the short development time, while the sensitivity of the resist is better in QSR-5D2 developer. These results are consistent with those of previous studies [39, 44, 45]. Furthermore, the sensitivity obtained for QSR-5 is relativity higher compared to most of the other e-resists that have been used for nanofabrication on unconventional surfaces [33–37].

RESULTS AND DISCUSSION

Mastering this QSR-5 electron sensitive negative resist allows performing micro and nanofabrication on suspended cantilever. We now show the integration of metallic films on suspended, non-planar AFM probe based on using the QSR-5 resist. It consists of several major steps such as thin film deposition, dry etching by reactive ion etching and ion beam etching, electron resists deposition, and electron beam lithography. The detailed description of the fabrication process is illustrated in Figure 5 (a) to (e).

The first step in this process is to install the AFM probe on a specific metal holder and fixed with a clamp to avoid electrical drift during the EBL. Thin films of titanium (Ti) and gold (Au) are deposited with thicknesses of 5 and 50 nm respectively using an electron gun evaporator. Gold was chosen to create electrical leads because of its excellent corrosion resistance and high electrical conductivity, and titanium film is used as an adhesion layer. Afterwards, QSR-5 e-resist is thermally evaporated at a chamber pressure of 2 $\times 10^{-7}$ mbar. Next, the electron exposure of a 800 nm wide strip is done on a pyramidal-shaped AFM tip with an accelerating voltage of 5 keV and an optimal dose of 400 μC.cm^{-2}. The e-beam lithography is done using a diaphragm aperture of 7.5 μm, a working distance of 8 μm giving a depth of focus larger than 10 μm, largely enough to expose non-planar surface like the pyramid of the tip of height 3 μm. Afterwards, the development is performed in QSR-5D2 developer. Since the dose required for complete exposure of the resist is about six times less as compared to MEK (as shown in Figure 4 (b)), this will help to expose the large area of the electrical pads dedicated to microbonding (as drawn in Figure 6 (d)). Then, the obtained

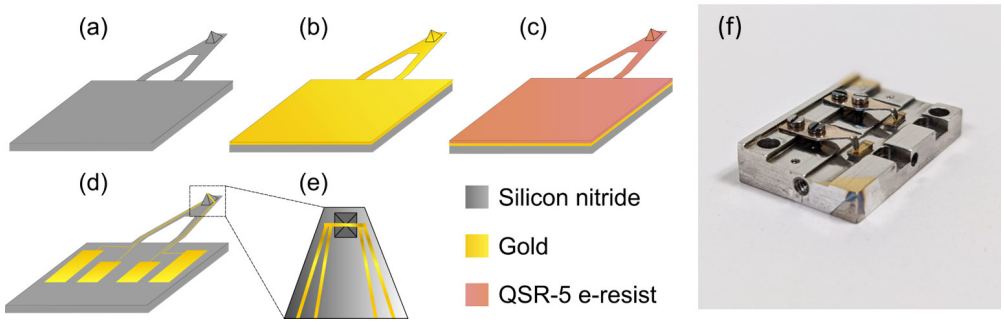

FIG. 5. Schematic illustration of the steps involved to integrate metallic thin films on non-planar 3D commercial AFM probes. (a) Silicon nitride (SiN) based AFM probe with thermal conductivity and electrically insulating properties. (b) Deposition of Ti/Au by e-gun evaporation with thicknesses of 5 and 50 nm respectively. (c) Thermal evaporation of QSR-5 negative e-resist with thickness of 170 nm. (d) E-beam lithography and development of resist; IBE process to define the electrical leads of Ti/Au on the AFM cantilever and chip. (e) Top-view of the patterned gold strip on the AFM tip. (f) A picture of the tip holder used during all the lithography processes: resist evaporation, EBL and etching procedures.

patterns of resist are used as a hard mask for dry etching of Ti/Au using IBE. The ion etching is carried out at a power of 400 W in Ar atmosphere with a pressure of 0.1 mTorr to remove Ti/Au layers from the unexposed area during the EBL. Finally, O_2 plasma is used to clean the resist residues from the AFM probe for two minutes.

Figure 6 (a) and (b) show the SEM images of the structured QSR-5 resist on the AFM tip with width of 800 nm and Figure 6 (c) and (d) demonstrate the well-defined patterning of Ti/Au film on the non-planar 3D AFM probe with a height of 3 μm via EBL and etching process only. The small protrusion on the apex of the tip comes from bigger rice grain structures (Figure 3 (a)) of QSR-5 that grow on the apex of the tip; this may sometimes affect the spatial resolution of the ecthing process at the apex. To avoid such tip effect due to the QSR-5 growth, EBL on the face of the pyramid will be preferred.

Next, the targeted application of our fabrication process is to integrate a niobium nitride resistive thermometer close to the apex of the AFM tip for scanning thermal measurements. As a temperature sensitive material, NbN thin films have been widely used for high-resolution temperature and thermal measurements over a broad temperature range from sub-Kelvin temperature in a dilution refrigerator to room temperature especially

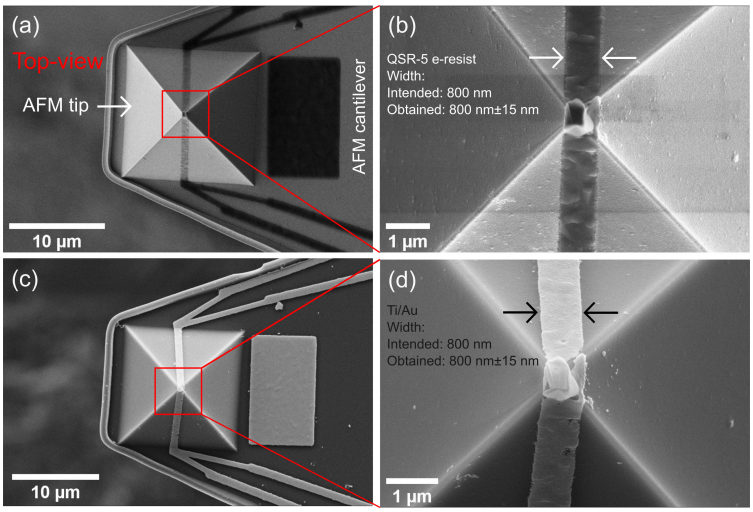

FIG. 6. SEM images of patterned QSR-5 resist on AFM probes by EBL and dry etching process, with increasing magnifications from (a) to (b). The electron energy and exposure dose of 5 keV and 400 μC.cm^{-2} are used respectively. QSR-5 is developed using QSR-5D2 developer for 12 minutes at 30 °C. (c) and (d) show the patterning of Au lines on AFM probe via performing the Ar plasma step inside Plassys IBE MU400 (2 sccm Ar gas, 0.1 mTorr pressure, and 400 W RF power).

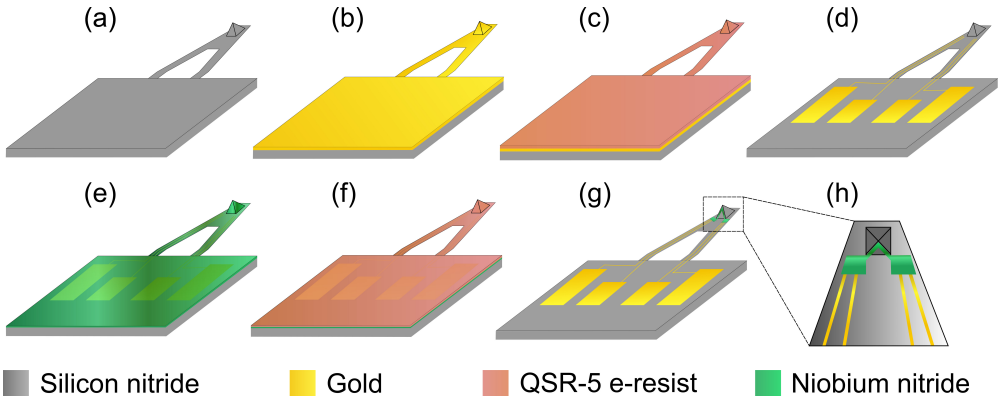

FIG. 7. Schematic representation of the steps involved to integrate thermal sensitive NbN thin films on non-planar AFM probes. (a) to (d) show the patterning of Au thin film for electrical contacts on the AFM cantilever, as described in the Figure 5. (e) Deposition of the NbN thin is carried out by DC-pulsed magnetron sputtering with thickness of 70 nm. (f) Evaporation of QSR-5 e-resist on the top of NbN. (g) Patterning of NbN thermometer via EBL and dry etching (SF_6 plasma). (h) Final design of SThM probe: top-view of the integrated NbN thin film at the apex of the tip and 4-terminal contact lines.

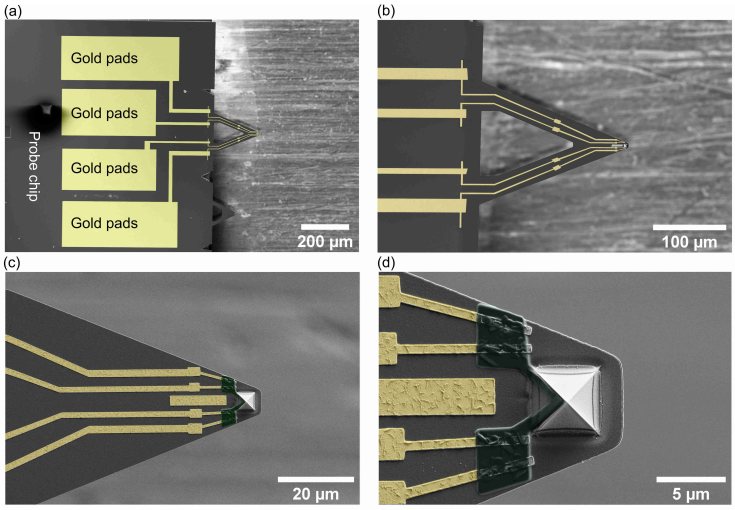

FIG. 8. SEM images illustrate the integration of the thermal sensitive NbN film on commercial AFM probes. (a) and (b) Top view of fabricated four-terminal electrical leads of Ti/Au (yellow, false colour) on AFM chip. (c) and (d) show the integration if NbN resistive thermometer (green, false colour) at the apex of the non-planar pyramidal shaped AFM tip.

for suspended systems [5, 46–50]. Combined with its low electrical thermal conductivity and a high resistance variation with temperature at 300 K, NbN is a very good candidate for room temperature as well as low temperature applications [46, 50]. Figure 7 illustrates the schematic representation of the full fabrication process involved for fabricating thermal probe including NbN thermometer on an AFM cantilever.

The NbN thermal probes dedicated to SThM will be constituted of four electrical leads, two for applying the current and two to measure the voltage, along with the NbN thermometer located in between the four contact leads. To define the electrical leads of Ti/Au on AFM cantilever and chip, we used the same fabrication steps as summarized in Figure 5 and detailed in Figure 7(a) to (d). The resultant patterned structures of Ti/Au are shown in Figure 7(d). After this step, the thin film NbN thermometer with a thickness of 70 nm is deposited by using DC-pulsed magnetron sputtering from a highly pure (99.95%) Nb target in the presence of Ar/N_2 gas (Figure 7(e); the detailed description of this step can be found in Ref. 46. After the NbN deposition, QSR-5 resist is deposited on top of the NbN thin film (Figure 7(f)) and structured again using EBL, followed by development via soaking in MEK developer at 30 °C for 90 seconds. Again, the obtained patterns of resist are used as a hard mask for the SF_6 plasma etching. Sharp patterns, as obtained when

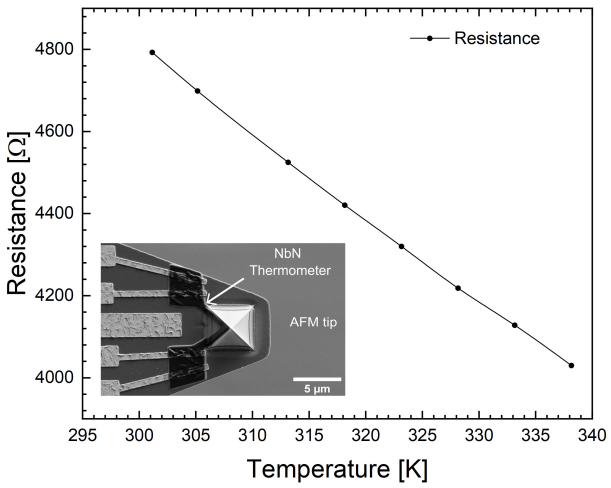

FIG. 9. Electrical resistance of the NbN thermometer located on the AFM tip (presented in the inset SEM image) measured using the four terminal electrical leads of Ti/Au as a function of temperature. The variation of the resistance shows the sensitivity to temperature of the NbN thermometer.

using MEK, are important for a good geometry definition of the NbN thermometers. The alignement of the second EBL as compared to the gold leads is made by a quick imaging of the end of the AFM cantilever fast enough not to expose the QSR-5 resist. Indeed, using MEK developper that requires higher electron dose is an advantage because it allows the realignment procedure by SEM image without risking to expose too much the resist. Finally, SF_6 plasma etching is carried out for achieving the precise and well-defined patterns of the NbN thermometer at the apex of the AFM tip as shown in Figure 7(g) and (h) where the NbN nanostructured thermometer is in green, the QSR-5 resist is used as a mask during the SF6 plasma.

The SThM tip, fabricated following that protocol, is shown in Figure 8 where in (a) we see the four pads dedicated to microbonding and in (b) and (c) the Ti/Au electrical leads converging towards the pyramid of the AFM probe; we are using false yellow color to clearly identify the Ti/Au lines. Figure 8 (d) is a zoom on the apex of the AFM probe, where the NbN thermometer is easily located using false green color. As a result, the NbN thermometer has been structured on one face of the pyramid demonstrating the powerness of the fabrication process based on evaporable electron sensitive QSR-5 resist.

In order to fully demonstrate the efficiency of this fabrication process, it is important to perform the electrical characterization of the NbN thermometer. This has been done by measuring the resistance of NbN thermometer on the AFM tip as a function of temperature. An example of such a temperature characterization is shown in Figure 9. It clearly shows the high potential of such a nanofabrication process of a thermal AFM probe for SThM measurements since a significant change of the NbN resistance is observed (13.5 Ohm per celsius degree). The best application of this thermal probe is either for the measurement of local temperature field when performing in contact scanning thermal microscopy or for the measurement of local thermal conductivity in an AFM environment.

CONCLUSIONS

In this work, we showed the lithographic capabilities of thermally evaporated QSR-5 e-resist with a combination of EBL technique and dry etching processes on planar and non-planar suspended surfaces. We achieved rectangular structures with few hundreds of nanometer width on planar or 2D surface. The impact of two different developers has been studied as a function of exposure doses. We found that the sensitivity of QSR-5 resist is improved when the development is performed in QSR-5D2 developer compared to MEK, the former will then be preferred for small dimension devices.

We demonstrated the efficiency of this e-beam sensitive resist by integrating nanofabricated electrical elements on highly non-planar 3D architectures: an AFM tip. In our results, we first demonstrated the patterning of Ti/Au thin film at the apex of the AFM probe. Secondly, we also showed that it is possible to integrate a highly sensitive NbN thermometer at the apex of an AFM tip. The nanofabrication of such new thermal measurement device can potentially enhance the sensitivity of SThM probes. Moreover, we are convinced that this innovative process will significantly contribute to ease the fabrication of novel nanostructures on suspended objects or non-planar surfaces. This advancement will substancially enhance the capability of developping suspended nano-sensors to explore various physical phenomena in novel devices and architectures at the nanoscale.

ACKNOWLEDGMENTS

The authors acknowledge fruitful discussions and insights provided by Jean-François Robillard and Pierre-Olivier Chapuis. We also thank the technical support provided by Nanofab, THEMA, Pôle électronique, Pôle de cryogénie facilities in Institut Néel.

The research leading to these results has received funding from the ANR TIPTOP grant No. ANR-16-CE09-0023, the European Union's Horizon 2020 Research and Innovation Programme, under grant agreement No. 824109, ANR project MESOPHON project grant agreement No. ANR-15-CE30-0019, and the Laboratoire d'excellence LANEF in Grenoble grant agreement No. ANR-10-LABX-51-01.

DATA AVAILABILITY STATEMENT

All data that support the findings of this study are included within the article. They will be available under reasonable request to the authors.

[1] I. Zardo and R. Rurali, Manipulating phonons at the nanoscale: Impurities and boundaries, Current Opinion in Green and Sustainable Chemistry **17**, 1 (2019).

[2] D. Tainoff, A. Proudhom, C. Tur, T. Crozes, S. Dufresnes, S. Dumont, D. Bourgault, and O. Bourgeois, Network of thermoelectric nanogenerators for low power energy harvesting, Nano Energy **57**, 804 (2019).

[3] D. Singhal, J. Paterson, M. Ben-Khedim, D. Tainoff, L. Cagnon, J. Richard, E. Chavez-Angel, J. J. Fernandez, C. M. Sotomayor-Torres, D. Lacroix, D. Bourgault, D. Buttard, and O. Bourgeois, Nanowire forest of pnictogen–chalcogenide alloys for thermoelectricity, Nanoscale **11**, 13423 (2019).

[4] E. Pop, Energy dissipation and transport in nanoscale devices, Nano Res. **3**, 147 (2010).

[5] A. Tavakoli, K. Lulla, T. Crozes, N. Mingo, E. Collin, and O. Bourgeois, Heat conduction measurements in ballistic 1d phonon waveguides indicate breakdown of the thermal conductance quantization, Nature Commun. **9**, 4287 (2018).

[6] M. Consales, A. Ricciardi, A. Crescitelli, E. Esposito, A. Cutolo, and A. Cusano, Lab-on-fiber technology: toward multifunctional optical nanoprobes, ACS Nano **6**, 3163 (2012).

[7] A. Grigorescu and C. Hagen, Resists for sub-20-nm electron beam lithography with a focus on hsq: state of the art, Nanotechnology **20**, 292001 (2009).

[8] H. Zhou, B. Chong, P. Stopford, G. Mills, A. Midha, L. Donaldson, and J. Weaver, Lithographically defined nano and micro sensors using "float coating" of resist and electron beam lithography, J. Vac. Sci. Techno., B: Microelectron. Process. Phenom. **18**, 3594 (2000).

[9] E. Sarajlic, R. Vermeer, M. Delalande, M. H. Siekman, R. Huijink, H. Fujita, and L. Abelmann, Batch fabrication of scanning microscopy probes for thermal and magnetic imaging using standard micromachining, in *23rd IEEE Inter. Conf. on MEMS* (IEEE, 2010) p. 328.

[10] B.-S. Yeo, J. Stadler, T. Schmid, R. Zenobi, and W. Zhang, Tip-enhanced raman spectroscopy–its status, challenges and future directions, Chem. Phys. Lett. **472**, 1 (2009).

[11] T. W. Johnson, Z. J. Lapin, R. Beams, N. C. Lindquist, S. G. Rodrigo, L. Novotny, and S.-H. Oh, Highly reproducible near-field optical imaging with sub-20-nm resolution based on template-stripped gold pyramids, ACS Nano **6**, 9168 (2012).

[12] J. Martin, N. Akerman, G. Ulbricht, T. Lohmann, J. v. Smet, K. Von Klitzing, and A. Yacoby, Observation of electron–hole puddles in graphene using a scanning single-electron transistor, Nature Phys. **4**, 144 (2008).

[13] A. Majumdar, Scanning thermal microscopy, Annu. Rev. Mater. Res. **29**, 505 (1999).

[14] K. Edinger, T. Gotszalk, and I. Rangelow, Novel high resolution scanning thermal probe, J. Vac. Sci. Techno., B: Microelectron. Process. Phenom. **19**, 2856 (2001).

[15] S. Lefevre, S. Volz, J.-B. Saulnier, C. Fuentes, and N. Trannoy, Thermal conductivity calibration for hot wire based dc scanning thermal microscopy, Rev. Sci. Instrum **74**, 2418 (2003).

[16] P. S. Dobson, J. M. Weaver, and G. Mills, New methods for calibrated scanning thermal microscopy (sthm), in *Proc. IEEE Sens.* (IEEE, 2007) p. 708.

[17] K. Kim, W. Jeong, W. Lee, and P. Reddy, Ultra-high vacuum scanning thermal microscopy for nanometer resolution quantitative thermometry, ACS Nano **6**, 4248 (2012).

[18] M. E. Pumarol, M. C. Rosamond, P. Tovee, M. C. Petty, D. A. Zeze, V. Falko, and O. V. Kolosov, Direct nanoscale imaging of ballistic and diffusive thermal transport in graphene nanostructures, Nano Lett. **12**, 2906 (2012).

[19] S. Gomès, A. Assy, and P.-O. Chapuis, Scanning thermal microscopy: A review, Phys. Stat. Sol. A **212**, 477 (2015).

[20] J. Bodzenta, J. Juszczyk, A. Kaźmierczak-Bałata, P. Firek, A. Fleming, and M. Chirtoc, Quantitative thermal microscopy measurement with thermal probe driven by dc+ ac current, Int. J. Thermophys **37**, 1 (2016).

[21] N. Mosso, U. Drechsler, F. Menges, P. Nirmalraj, S. Karg, H. Riel, and B. Gotsmann, Heat transport through atomic contacts, Nature Nanotechnol. **12**, 430 (2017).

[22] L. Cui, W. Jeong, S. Hur, M. Matt, J. C. Klöckner, F. Pauly, P. Nielaba, J. C. Cuevas, E. Meyhofer, and P. Reddy, Quantized thermal transport in single-atom junctions, Science **355**, 1192 (2017).

[23] A. Massoud, J.-M. Bluet, V. Lacatena, M. Haras, J.-F. Robillard, and P.-O. Chapuis, Native-oxide limited cross-plane thermal transport in suspended silicon membranes revealed by scanning thermal microscopy, J. Appl. Phys **111**, 063106 (2017).

[24] Y. Zhang, W. Zhu, F. Hui, M. Lanza, T. Borca-Tasciuc, and M. Muñoz Rojo, A review on principles and applications of scanning thermal microscopy (sthm), Adv. Funct. Mater. **30**, 1900892 (2020).

[25] G. Pernot, A. Metjari, H. Chaynes, M. Weber, M. Isaiev, and D. Lacroix, Frequency domain analysis of 3ω-scanning thermal microscope probe—application to tip/surface thermal interface measurements in vacuum environment, J. Appl. Phys **129**, 055105 (2021).

[26] K. Yamazaki and H. Yamaguchi, Electron beam lithography on vertical side faces of micrometer-order si block, J. Vac. Sci. Techno., B: Microelectron. Process. Phenom. **30**, 041601 (2012).

[27] J. Linden, C. Thanner, B. Schaaf, S. Wolff, B. Lägel, and E. Oesterschulze, Spray coating of pmma for pattern transfer via electron beam lithography on surfaces with high topography, Microelectron. Eng. **88**, 2030 (2011).

[28] I. Peterson, Langmuir-blodgett electron-beam resists, IEEE Proc.-I: Solid-State Electron Devices I **130**, 252 (1983).

[29] R. K. Dey, F. Aydinoglu, and B. Cui, Electron beam lithography on irregular surface using grafted pmma monolayer as resist, Adv. Mater. Interfaces **4**, 1600780 (2017).

[30] H. Yamada, F. Aydinoglu, Y. Liu, R. K. Dey, and B. Cui, Single layer surface-grafted pmma as a negative-tone e-beam resist, Langmuir **33**, 13790 (2017).

[31] F. Aydinoglu, H. Yamada, R. K. Dey, and B. Cui, Grafted polystyrene monolayer brush as both negative and positive tone electron beam resist, Langmuir **33**, 4981 (2017).

[32] R. Glass, M. Arnold, J. Bluemmel, A. Kueller, M. Moeller, and J. P. Spatz, Micro-nanostructured interfaces fabricated by the use of inorganic block copolymer micellar monolayers as negative resist for electron-beam lithography, Adv. Funct. Mater. **13**, 569 (2003).

[33] G. M. King, G. Schürmann, D. Branton, and J. A. Golovchenko, Nanometer patterning with ice, Nano Lett. **5**, 1157 (2005).

[34] A. Han, D. Vlassarev, J. Wang, J. A. Golovchenko, and D. Branton, Ice lithography for nanodevices, Nano Lett. **10**, 5056 (2010).

[35] A. Han, A. Kuan, J. Golovchenko, and D. Branton, Nanopatterning on nonplanar and fragile substrates with ice resists, Nano Lett. **12**, 1018 (2012).

[36] D. Zhao, A. Han, and M. Qiu, Ice lithography for 3d nanofabrication, Sci. Bull. **64**, 865 (2019).

[37] J. Zhang, C. Con, and B. Cui, Electron beam lithography on irregular surfaces using an evaporated resist, ACS Nano **8**, 3483 (2014).

[38] G. Zharik, S. Dagesyan, E. Soldatov, D. Presnov, and V. Krupenin, Nanometer scale lithography with evaporated polystyrene, Moscow University Physics Bulletin **72**, 627 (2017).

[39] E. Lavallee, J. Beauvais, D. Drouin, M. Cloutier, L. Mun, Y. Awad, H. Smith, M. Lim, J. Carter, and M. Schattenburg, Evaporated electron beam sensitive organic resist for the back-patterning of x-ray lithography masks, in *2002 MNC, 2002. Digest of Papers.* (IEEE, 2002) p. 320.

[40] S. Ma, C. Con, M. Yavuz, and B. Cui, Polystyrene negative resist for high-resolution electron beam lithography, Nanoscale Res. Lett. **6**, 1 (2011).

[41] L. Shi, O. Kwon, A. C. Miner, and A. Majumdar, Design and batch fabrication of probes for sub-100 nm scanning thermal microscopy, J. Microelectron. Syst. **10**, 370 (2001).

[42] The cantilevers are bruker ^{TM} otr8-10.

[43] R. Legario, P. Kelkar, J. Beauvais, E. Lavallée, D. Drouin, M. Cloutier, D. Turcotte, P. Yang, L. Mun, Y. Awad, and P. Lafrance, Nano patterning on fragile or 3D surfaces with sterol based vapour deposited electron beam resist, Avances in Resist technology and Processing XXI, SPIE **5376** (2004).

[44] P. Kelkar, J. Beauvais, E. Lavallee, D. Drouin, M. Cloutier, D. Turcotte, P. Yang, L. K. Mun, R. Legario, Y. Awad, *et al.*, Nano patterning on optical fiber and laser diode facet with dry resist, J. Vac. Sci. Technol. A **22**, 743 (2004).

[45] J.-C. Gerbedoen, A. Aliane, A. Giguère, D. Drouin, R. Ares, and V. Aimez, All evaporation submicron lift-off lithography process with negative e-beam qsr-5 resist, Microelectron. Eng. **103**, 123 (2013).

[46] O. Bourgeois, E. André, C. Macovei, and J. Chaussy, Liquid nitrogen to room-temperature thermometry using niobium nitride thin films, Rev. Sci. Instrum. **77**, 126108 (2006).

[47] J. Heron, T. Fournier, N. Mingo, and O. Bourgeois, Mesoscopic size effects on the thermal conductance of silicon nanowire, Nano Lett. **9**, 1861 (2009).

[48] E. Dechaumphai and R. Chen, Sub-picowatt resolution calorimetry with niobium nitride thin-film thermometer, Rev. Sci. Instrum. **85**, 10.1063/1.4895678 (2014).

[49] H. Ftouni, C. Blanc, D. Tainoff, A. D. Fefferman, M. Defoort, K. J. Lulla, J. Richard, E. Collin, and O. Bourgeois, Thermal conductivity of silicon nitride membranes is not sensitive to stress, Phys. Rev. B **92**, 125439 (2015).

[50] T. Nguyen, A. Tavakoli, S. Triqueneaux, R. Swami, A. Ruhtinas, J. Gradel, P. Garcia-Campos, K. Hasselbach, A. Frydman, B. Piot, *et al.*, Niobium nitride thin films for very low temperature resistive thermometry, J. Low Temp. Phys. **197**, 348 (2019).